WILEY-VCH

COMMUNICATION

Enhanced N$_2$ fixation activity by converting Ti$_3$C$_2$ MXenes nanosheets to nanoribbons

Hua Wei [a, c], #, Qian Jiang [b], #, Claudio Ampelli [a], Shiming Chen [b], Siglinda Perathoner [a], Yuefeng Liu [b],* and Gabriele Centi [a],*

[a]	Dr. H. Wei, prof. C. Ampelli, prof. S. Perathoner, prof. G. Centi Dept.s ChimBioFarAm and MIFT, V.le F. Stagno D'Alcontres 31, 98166 Messina, Italy. E-mail: centi@unime.it
[b]	Dr. Q. Jiang, Dr. S. Chen, prof. Y. Liu Dalian National Laboratory for Clean Energy, Dalian Institute of Chemical Physics, Chinese Academy of Sciences, 457 Zhongshan Road, Dalian 116023, China. E-mail: yuefeng.liu@dicp.ac.cn
[c]	Dr. H. Wei University of Lyon, Institut de Chimie de Lyon, UMR 5265 – CNRS – Université Lyon 1, ESCPE Lyon, Laboratoire de Chimie, Catalyse, Polymères et Procédés (C2P2), Equipe Chimie Organométallique de Surface, Villeurbanne, France
[#]	These authors contributed equally to this work.
	Supporting information for this article is given via a link at the end of the document.

Abstract: Metal carbides M$_2$C (MXenes) with two-dimensional (2D) structure have been indicated as promising materials for N$_2$ fixation, with the activity related to edge planes. We demonstrate instead here that the transformation from a 2D (nanosheets) to a 3D-type nanostructure (nanoribbons), leads to a significant enhancement of the N$_2$ fixation activity, due to the formation of exposed Ti-OH sites. A linear relationship is observed between ammonia formation rate and amount of oxygen on the surface of Ti$_3$C$_2$ MXene.

MXenes are metal carbide or nitride materials with a two-dimensional (2D) structure, which attracted a large interest recently for a broad range of applications such as materials for energy and environmental applications,[1-4] and catalysis.[5-7] In the latter area, several papers deal on N$_2$ fixation (NRR),[8-18] a topic of current large interest to directly produce ammonia from nitrogen.[19] Mxene presents the unusual electronic property of the 2D structure and also the unique property of transition metal carbides, such as metallic conductivity, and the hydrophilic nature of their hydroxyl or oxygen terminated surfaces. For these properties there is a large interest on the use of Mxenes as novel NRR electrocatalysts, as emerges also from the state-of-the-art comparison of NRR electrocatalysts (see Supplementary Info). They have properties well comparable with those of the best reported NRR electrocatalysts, with the advantage of a flexible way to tune further their properties, and thus a large potential for further improvement.

Most of studies on MXenes as NRR materials indicated the need to have a 2D nanostructure, with the activity in N$_2$ fixation attributed generally to edge sites of the nanosheets. Luo et al.,[16] for example, indicate the middle Ti at the edge sites as the active sites for NRR. The mechanism proposed involved hydrogenation of undissociated N$_2$ molecules. Gouveia et al.[6] considered instead that N$_2$ dissociation occurs easily on the MXene (0001) surface. The top site above the metal ions on the surface of MXene nanosheets was also indicated by Wang et al.[8] as the sites for end-on adsorption of N$_2$ which is then hydrogenated, rather than

dissociated. Johnson et al.[15] indicated that edge sites of MXene are involved in NRR reaction and that F functional groups enhance the NRR performance in comparison to O functional groups. Xia et al.,[11] on the contrary, indicated that exposed Ti sites in Ti$_3$C$_2$OH facilitate the electron transfer and promote the adsorption and activation of dinitrogen. Guo et al.[12] suggested that OH terminal groups of MXene are inactive, indicating thus that a modification of the surface chemical states by introducing Fe heteroatoms is necessary to increase the activity.

Most of the studies based their conclusions mainly on theoretical modelling. However, notwithstanding the discordances in the nature of the active MXene materials for NRR reaction, a common agreement is that a 2D configuration is needed.

2D-type materials are an area of intense research interest for a number of applications in the field of materials for energy, including catalysis.[20] On the other hand, it is possible to assemble and master 2D materials to form other type of 3D-like nanomaterials.[21] MXenes nanosheets can be subjected to a transformation from a 2D to a 3D-like nanostructures.[22] This will allow to clarify the relationship between performances and type of nanostructure. In the specific case of NRR, this method of manipulating nanostructures allows to understand the role and relevance of the presence of a 2D nanostructure on edge or planar bases, by comparing the behaviour of very analogous materials, but having a different nanoshape.

We have thus investigated how the conversion of Ti$_3$C$_2$ nanosheets to 3D-like nanoribbons influence the properties and NRR reactivity to obtain insights about the role of the nanostructure in this reaction providing therefore elements for theoretical modelling to overcome the present discordances on the nature of the active materials and thus allow their better design.

Ti$_3$C$_2$ MXene nanosheets (MNSs) were prepared by HF etching (in 40% HF solution for 72h) of Ti$_3$AlC$_2$ starting precursor, followed by centrifugation, washing and drying at 60°C. The obtained MNSs are then treated in 6 M KOH for 72h (sealed container under Ar atmosphere), followed by steps as above.
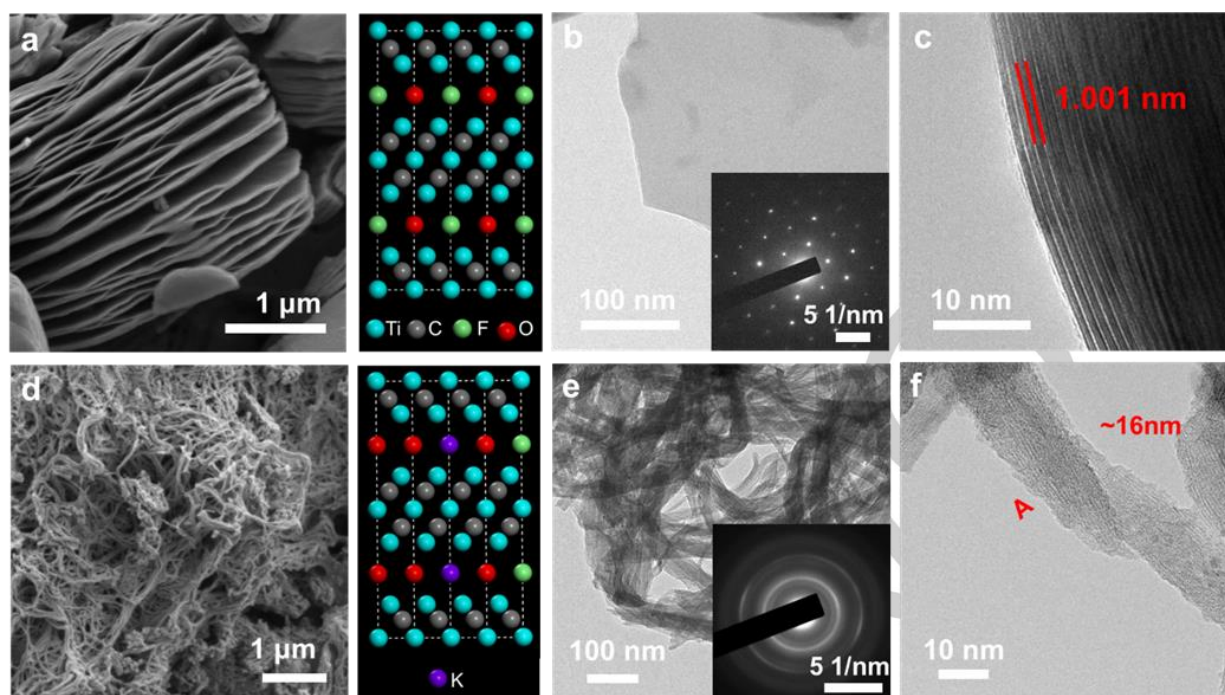
Figure 1 (a) SEM images of Ti$_3$C$_2$ MNSs (b) Top-view TEM images and electron diffraction patterns of Ti$_3$C$_2$ MNSs. (c) Cross-sectional TEM images of Ti$_3$C$_2$ MNSs. (d) SEM images of Ti$_3$C$_2$ MNRs. (e) TEM images of Ti$_3$C$_2$ MNRs and electron diffraction patterns of Ti$_3$C$_2$ MNRs. (f) HRTEM images of Ti$_3$C$_2$ MNRs, a single MNR with a width of ~ 16 nm, taken from the A position.

Ti$_3$C$_2$ MXene nanoribbons (MNRs) are obtained in this way. The method of preparation is analogous to that used by Lian et al.[23] MNSs and MNRs were dispersed in ethanol containing 10% Nafion (ultrasonic mixing for 90 min), obtaining an homogenous ink which is then deposited by spray drying onto a gas-diffusion layer (GDL). The GDL with the deposited electrocatalyst is then hot pressed to a Nafion membrane. The electrocatalyst is located at the interface between the Nafion membrane and the GDL. The loading of the electrocatalyst resulted 0.2 mg/cm^{-2}.

The electrodes were tested in an electrocatalytic flow reactor, where the hemi-cell for NRR reaction operates without a liquid electrolyte. This type of electrocatalytic reactor is different from the conventional electrocatalytic reactors operating with the electrodes immersed in a liquid electrolyte. The reason is to avoid issues related to low N$_2$ solubility in the electrolyte, and to allow an easier recovery of the ammonia produced. In fact, NH$_3$ is recovered directly from the gas outlet of the flow reactor. Details on the preparation of the electrodes, although by using different type of electrocatalysts, and on the characteristics of the electrocatalytic reactor were reported earlier.[24-26] Supplementary Info reports also details about the flow electrocatalytic reactor, the experimental procedure of testing, the determination of ammonia and other possible products, and the series of control experiments made to verify that ammonia derives effectively from the electrocatalytic reduction of N$_2$.

The scanning electron microscopy (SEM) images (Figure 1a) for Ti$_3$C$_2$T$_x$ (where T= F, OH) after the HF etching, show a MXene loosely layered 2D structure, indicating the successful exfoliation of Al from the MAX phase (Ti$_3$C$_2$Al). The transparency of the nanosheet presented in Figure 1b suggests that the likely presence of single layer sheet having a thickness of around 200 nm.[27] It is present a monocrystal as shown by diffraction pots of the selected area electron diffraction (SAED) reported in the inset

of Figure 1b. The HRTEM image (Figure 1c) shows the interlayer spacing of 1.00 nm corresponding to the (002) plane,[28] which is consistent with the value measured by XRD and with results obtained by Ghidiu et al.[29] After Ti$_3$C$_2$ nanosheets treatment by KOH, nanoribbons could be well evidenced (Figure 1d). The nanoribbons have a diameter around 16 nm, in agreement also with HRTEM images (Figures 1e and 1f).
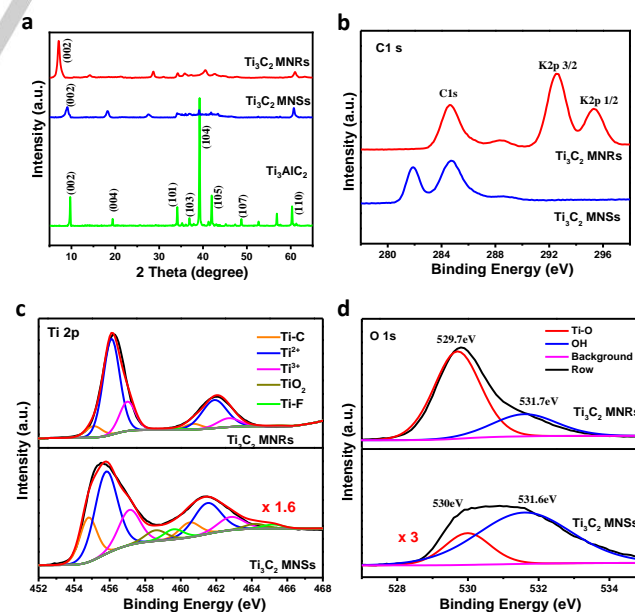
Figure 2 Structural characterization of Ti$_3$C$_2$ MNRs, Ti$_3$C$_2$ MNSs, and pristine Ti$_3$AlC$_2$. (a)XRD patterns of Ti$_3$C$_2$ MNRs, Ti$_3$C$_2$ MNSs, and pristine Ti$_3$AlC$_2$. (b-d) XPS spectra of Ti$_3$C$_2$ MNRs and Ti$_3$C$_2$ MNSs in the (b) C 1s, (c) O1s (d) Ti 2p, regions

COMMUNICATION

The conversion of Ti_3AlC_2 (MAX phase) to Ti_3C_2 MNSs and MNRs is confirmed by X-ray diffraction (XRD) (Figure 2a). Compared with the pattern of Ti_3AlC_2, the most intense peak (104) of Ti_3AlC_2 disappears and the (002) reflection of MXene shifts from 9.7° to 9.1° broadening at the same time. This is consistent with the expected interlayer spacing expansion in passing from Ti_3AlC_2 to Ti_3C_2 MNSs.[30] When the Ti_3C_2 MNSs is further treated in KOH solution, the (002) reflection shifts to 7.1° and further broaden, consistently with the further expansion of interlayer spacing.[23]

The full spectrum XPS and associated elemental analysis (Supplementary Info, Figure S3) confirm the existence of C, K, O and F in Ti_3C_2 MNRs. It also evidenced the large enhancement of the O content which becomes over twice the initial value after the KOH treatment, indicating that the nanoribbon edges are rich in OH groups.

In the C 1s region (Figure 2b), the characteristic peaks of $K2p_{3/2}$ at 292.4 eV and $K2p_{1/2}$ at 295.2 eV are present only in Ti_3C_2 MNRs, but K presence was not detected in Ti_3C_2 MNSs neither in Ti_3AlC_2. This is consistent with XPS elemental analysis (Supplementary Info, Figure S3b). This accounts for the alkalization of MNRs, consistent with XRD measurement. However, the K atoms do not enter in the Ti_3C_2 MNRs structure to occupy the anion sites, as confirmed by analysis of the lattice spacing of (002) plane in XRD diffractograms.

After the treatment by KOH, the intensity of the XPS Ti-F peaks decreased markedly (Supplementary Info, Figure S3), while the contents of -OH on the surface increases significantly, indicating that a large amount of -F terminal groups were replaced by hydroxyl groups and consequently the formation of O-terminated Ti_3C_2 MNRs.[31] EDX analysis of Ti_3C_2 MNSs and Ti_3C_2 MNR samples confirm this indication (Supplementary Info, Figure S4). The comparison of the elemental composition by XPS and EDX (SEM) (Supplementary Info, Figures S3 and S4, respectively) show that after the treatment by KOH, the Ti/C ratio increases owing to the carbon corrosion by KOH. Being XPS detecting the surface composition with a depth less than about 5 nm while the detection depth for SEM is up to about 1μm, the comparison of Ti/C ratios measured by XPS and EDX indicates a preferential surface carbon removal by the KOH treatment. The EDX of MAX phase (Ti_3AlC_2) and Ti_3C_2 MNSs (Supplementary Info, Table S1) indicates also that the oxygen content is similar in these two samples.

Figure 2c and 2d report the XPS Ti_{2p} and O_{1s} regions for the Ti_3C_2 MNRs (top) and MNSs (bottom) samples, respectively. Deconvolution of the spectra is also reported according to Lian et al.[23] and Halim et al.[32] For Ti_{2p} region, spectra were deconvoluted for Ti-C, Ti^{2+}, Ti^{3+} and TiO_2 components, while for O_{1s} region spectra were deconvoluted in Ti-O and -OH components. Figure 2c well indicates that the relative content of TiC decreased after KOH treatment with part of TiC transformed into Ti^{2+} and Ti^{3+}. This result is well consistent with the increase of O content commented before. Ti-F component also disappears after the MNSs to MNRs conversion. Figure 2d evidences that the conversion leads to a significant increase in the Ti-O component (note that the spectra of Ti_3C_2 MNSs are multiplied by a factor three in intensity).

The electrocatalytic measurements (at room temperature and ambient pressure) were performed in the flow reactor described before operating without a liquid electrolyte in the hemicell where the NRR reaction occurs. The flow of highly pure N_2 (further purified by passing through filters to capture eventual presence of NO_x, NH_3 and other possible contaminants) is passed through the

electrocatalytic hemicell with the ammonia formed being then recovered from the gas outlet stream by absorption in a 0.001 M H_2SO_4 solution. The amount of ammonia formed was detected by a spectrophotometric method reported in detail in the Supplementary Info. This method is highly sensitive and we consider preferable and more reliable with respect to alternative methods such as NMR, ion-selective electrodes or mass spectrometry (see Supplementary Info). Supplementary Info also describes the tests made to exclude the formation of hydrazine (N_2H_4) under our experimental conditions. The protons/electrons for the NRR reactions derive from water electrolysis occurring in the other hemicell of the electrocatalytic reactor. A Nafion membrane separates the two hemicells (see Supplementary Info).

A series of control tests were made to verify that ammonia forms from the N_2 present in the flowing gas-phase and not from other N-contaminants (see Supplementary Info). These tests include monitoring the change in ammonia formation by switching from N_2 to Ar or using labelled nitrogen. By feeding $N_2 + H_2$ at open circuit conditions, it was also verified that the catalytic activity (i.e. not related to electrocatalysis) was negligible. Figure S2 in the Supplementary Info reports the experimental protocol for NRR tests used in these experiments, to demonstrate that the detected NH_3 derives from the electrocatalytic reduction of N_2.

Based on cyclic voltammetry (CV) tests (Figure S6 in the Supplementary Info), we selected three voltages (in the range from -0.2V to -0.8V vs RHE) to screen the behaviour of Ti_3C_2 MNRs. Results are reported in Figure S7 and S8 (Supplementary Info). The highest NH_3 yield was obtained at −0.5 V vs RHE. Current density at this voltage is about -1.5 μA and remain stable for at least 3h of continuous tests. The current density remains stable also in longer term tests (up to about 10h), showing that the electrocatalyst is stable under these experimental conditions. This result was also in well agreement with CV tests (see Supplementary Info). At more negative voltage (-0.8 V), the current density instead decreases from the initial -3.5 μA value to about -4.5 μA (after 2h), indicating thus an in-situ transformation during the electrocatalytic tests. At a voltage of -0.2 V, the current density (about -0.5 μA) is instead low, indicating low catalytic activity. Further tests were thus made at -0.5 V. Data reported refer to the behaviour determined after 3h of continuous tests.
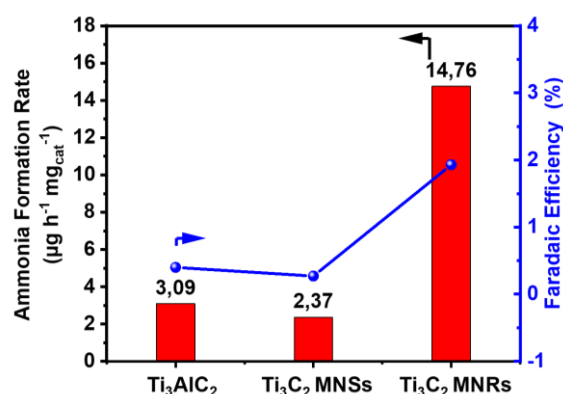

Figure 3 Ammonia formation rate and Faradaic efficiency with different electrodes at −0.5 V vs. RHE after 3 h of electrocatalytic tests at room temperature and ambient pressure.

Figure 3 reports the comparison of the rate of ammonia formation per mg of electrocatalysts for the pristine Ti_3AlC_2 sample, and Ti_3C_2 MNSs and MNRs samples. Pristine Ti_3AlC_2 and Ti_3C_2

MNSs have a quite comparable low activity in NRR, while Ti_3C_2 MNRs show a more than 5 times higher activity. Faradaic efficiency also increases to about 2% after transformation to nanoribbon. A stable current density was shown for all samples, indicating a stable behaviour at the applied voltage at least for 3h of continuous tests. No significant changes in the sample characteristics were also observed by electron microscopy, XPS and XRD characterization of these materials after the electrocatalytic tests (see Supplementary Info, Figure S7 and S8). The constant CV data during extended cycles also confirm this stability. These results thus show that morphological, structural, surface and reactivity characteristics of Ti_3C_2 MNRs remain unchanged at least for 10h of continuous electrocatalytic tests at -0.5V vs. RHE.

A linear relationship could be observed between the rate of ammonia formation in the three samples reported in Figure 3 and the amount of oxygen on the surface (atomic %) as detected by XPS measurements (Figure 4), suggesting a relationship between these two aspects.
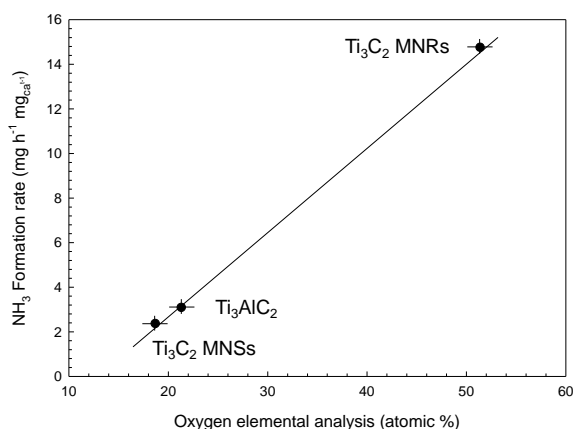
Figure 4 Relationship between ammonia formation rate at −0.5 V vs. RHE and atomic % of oxygen in the surface as measured by XPS.

The relationship presented in Figure 4 agrees (among others) with (i) Xia et al.[11] indications that exposed Ti sites (Ti_3C_2OH) are responsible for the improved electron transfer, adsorption and activation of dinitrogen, (ii) theoretical results of Tang et al.[33] that exposed Ti atom close to extra oxygen vacancy are responsible for activity in (defective) MXenes electrocatalysts, (iii) Jin et al.[34] indications that OH-rich MXenes (Ti_3C_2OH) show high NRR performances and (iv) Xia et al.[35] result that surface hydroxyl modification of MXene Ti_3C_2 facilitates the electron transfer and the adsorption and activation of dinitrogen. Therefore, this work shows that the transformation from a 2D-like morphology (nanosheets) to a 3D-like morphology (nanoribbons) leads to a large improvement in the NRR activity, due to an enhanced formation of active sites (likely Ti_3C_2OH) not blocked by F atoms.

To compare these data with literature, Table S2 in Supplementary Info reports a comparison of reaction conditions, ammonia formation rate and Faradaic selectivity of selected state-of-the-art literature results on NRR, organized in four classes of electrocatalytic materials: (a) MXenes, (b) modified and composite electrocatalysts based on MXenes, and electrocatalysts based on (c) noble metals or (d) transition metal oxides/sulphide. The comparison shows that particularly with respect to MXenes electrocatalysts, the electrocatalysts reported

here well compares with other published, taking into account of the differences in the operative conditions, and the use here of an electrocatalytic reactor without liquid electrolyte differently from the other cases. Note, in addition, that the scope in this work is not to show record performances, but instead to analyse the role of the conversion from 2D (nanosheet) to 3D-like (nanoribbon) morphology in Ti_3C_2 MXenes.

For a further comparison, some selected results will be compared here. Luo et al.[16] reported for MXene ($Ti_3C_2T_x$) nanosheets a maximum Faradic efficiency of 4.62% and a NH_3 yield rate of 2.7 $\mu g \cdot h^{-1} \cdot mg_{CAT}^{-1}$ at a best potential of -0.1 vs. RHE. Xia et al.[11] indicated as best performances (Ti_3C_2 with an increased amount of surface hydroxyl moieties) a yield rate of NH_3 of 1.71 $\mu g \cdot h^{-1} \cdot cm^{-2}$ with a Faradaic efficiency of about 7%. These performances were in line with those indicated for analogous samples in the reviews by Sun et al.[36] and Li and Wu.[37] We may thus conclude that data reported in Figures 3 and 4 are in line with those earlier reported for Ti_3C_2 nanosheet-type materials, and thus the results reported here evidence a significant enhancement in NRR activity passing from nanosheet to nanoribbon-type morphology. This is related to the formation of OH-rich Ti_3C_2 MXene. This is in agreement with previous literature indications and theoretical studies, but here is for the first time demonstrated the presence of a linear relationship between ammonia formation rate and amount of oxygen on the surface of Ti_3C_2 MXene.

Conclusions

This result evidences that a 2D (nanosheet) morphology is not necessary in MXene materials to show NRR activity, and a different morphology (nanoribbon), not having the same basal planes and type of edges, show instead an about five-time higher NRR activity. Characterization data indicate that in nanoribbon morphology, there is a preferential formation of exposed Ti-O sites, which various studies have indicated as responsible for improved electron transfer, adsorption, and activation of dinitrogen.[11,34,35] Present data agree with this interpretation, and evidence for the first time the presence of a linear relationship between ammonia formation rate and amount of oxygen on the surface of Ti_3C_2 MXene.

Acknowledgements

References

[1] J. Li, C. Guo, C. M. Li, *ChemSusChem* **2020**, *13*, 1047.

[2] R. Fang, C. Lu, A. Chen, K. Wang, H. Huang, Y. Gan, C. Liang, J. Zhang, X. Tao, Y. Xia, W. Zhang, *ChemSusChem* **2020**, *13*, 1409.

[3] X. Zhan, C. Si, J. Zhou, Z. Sun, *Nanoscale Horizons* **2020**, *5*, 235.

[4] J. Pang, R. G. Mendes, A. Bachmatiuk, L. Zhao, H. Q. Ta, T. Gemming, H. Liu, Z. Liu, M. H. Rummeli, *Chem. Soc. Rev.* **2019**, *48*, 72.

[5] T. A. Le, N. Q. Tran, Y. Hong, M. Kim, H. Lee, *ChemSusChem* **2020**, *13*, 945.

[6] J. D. Gouveia, A. Morales-Garcia, F. Vines, F. Illas, J. R. B. Gomes, *Appl. Catal. B*, **2020**, *260*, 118191.

[7] Z. Fu, N. Wang, D. Legut, C. Si, Q. Zhang, S. Du, T. C. Germann, J. S. Francisco, R. Zhang, *Chem. Rev.*, **2019**, *119*, 11980.

[8] A. Liu, Y. Yang, X. Ren, Q. Zhao, M. Gao, W. Guan, F. Meng, L. Gao, Q. Yang, T. Ma, X. Liang, *ChemSusChem* **2020**. Accepted DOI:10.1002/cssc.202000487.

[9] (a) S. Wang, B. Li, L. Li, Z. Tian, Q. Zhang, L. Chen, X. C. Zeng, *Nanoscale*, **2020**, *12*, 538Y. (b) Cheng, J. Dai, Y. Song, Y. Zhang, *Nanoscale*, **2019**, *11*, 18132.

[10] J. D. Gouveia, A. Morales-Garcia, F. Vines, J. R. B. Gomes, F. Illas, *ACS Catal.*, **2020**, *10*, 5049.

[11] J. Xia, S.-Z. Yang, B. Wang, P. Wu, I. Popovs, H. Li, S. Irle, S. Dai, H. Zhu, *Nano Energy*, **2020**, *72*, 104681,

[12] Y. Guo, T. Wang, Q. Yang, X. Li, H. Li, Y. Wang, T. Jiao, Z. Huang, B. Dong, W. Zhang, J. Fan, C. Zhi, *ACS Nano* **2020**, DOI: 10.1021/acsnano.0c04284

[13] L. Huang, X. Gu, G. Zheng, *Chem*, **2019**, *5*, 15.

[14] Y. Gao, Y. Cao, H. Zhuo, X. Sun, Y. Gu, G. Zhuang, S. Deng, X. Zhong, Z. Wei, X. Li, J.-g. Wang, *Catal. Today*, **2020**, *339*, 120.

[15] L. R. Johnson, S. Sridhar, L. Zhang, K. D. Fredrickson, A. S. Raman, J. Jang, C. Leach, A. Padmanabhan, C. C. Price, N. C. Frey, A. Raizada, V. Rajaraman, S. A. Saiprasad, X. Tang, Al. Vojvodic, *ACS Catal.*, **2020**, *10*, 253.

[16] Y. Luo, G.-F. Chen, L. Ding, X. Chen, L.-X. Ding, H. Wang, *Joule*, **2019**, *3*, 279.

[17] J. Zhao, L. Zhang, X.-Y. Xie, X. Li, Y. Ma, Q. Liu, W.-H. Fang, X. Shi, G. Cui, X. Sun, *J. Mater. Chem. A*, **2018**, *6*, 24031.

[18] X. Wen, J. Guan, *Nanoscale* **2020**, *12*, 8065.

[19] M. Shao, W. Shao, W. Chen, K. L. Ao, R. Tong, Q. Zhu, I. N. Chan, W. F. Ip, X. Shi, H. Pan, *Phys. Chem. Chem. Phys.*, **2018**, *20*, 14504.

[20] C. J. Heard, J. Čejka, M. Opanasenko, P. Nachtigall, G. Centi, S. Perathoner, *Adv. Mater.*, **2019**, *31*, 1801712.

[21] G. Centi, S. Perathoner, *Coord. Chem. Rev.*, **2011**, *255*, 1480-1498.

[22] Z. Wu, T. Shang, Y. Deng, Y. Tao, Q.-H. Yang, *Adv. Sci.*, **2020**, *7*, 1903077.

[23] P. Lian, Y. Dong, Z.-S. Wu, S. Zheng, X. Wang, S. Wang, C. Sun, J. Qin, X. Shi, X. Bao, *Nano Energy*, **2017**, *40*, 1.

[24] S. Chen, S. Perathoner, C. Ampelli, C. Mebrahtu, D. Su, G. Centi, *Angew. Chemie Int. Ed.*, **2017**, *56*, 2699.

[25] S. Chen, S. Perathoner, C. Ampelli, C. Mebrahtu, D. Su, G. Centi, *ACS Sustainable Chem. & Eng.*, **2017**, *5*, 7393.

[26] (a) S. Chen, S. Perathoner, C. Ampelli, H. Wei, S. Abate, B. Zhang, G. Centi, *J. Energy Chem.*, **2020**, *49*, 22. (b) S. Chen, S. Perathoner, C. Ampelli, H. Wei, S. Abate, B. Zhang, G. Centi, *ChemElectroChem*, **2020**, DOI:10.1002/celc.202000741

[27] M. Alhabeb, K. Maleski, T. S. Mathis, A. Sarycheva, C. B. Hatter, S. Uzun, A. Levitt, Y. Gogotsi, *Angew. Chem. Int. Ed.*, **2018**, *57*, 5444.

[28] J. B. Li, D. Yan, S. J. Hou, Y. Q. Li, T. Lu, Y. F. Yao, L. K. Pan, *J. Mater. Chem. A*, **2018**, *6*, 1234.

[29] M. Ghidiu, M. R. Lukatskaya, M. Q. Zhao, Y. Gogotsi, M. W. Barsoum, *Nature*, **2014**, *516*, 78.

[30] O. Mashtalir, M. Naguib, V, N. Mochalin, Y. Dall'Agnese, M. Heon, M. W. Barsoum, Y. Gogotsi, *Nature Comm.*, **2013**, *4*, 1716.

[31] J. Li, X. Yuan, C. Lin, Y. Yang, L. Xu, X. Du, J. Xie. J. Lin, J. Sun, *Adv. Energy Mat.*, **2017**, *7*, 1602725.

[32] J, Halim, K. M. Cook, M. Naguib, P. Eklund, Y. Gogotsi, J. Rosen, M.W. Barsoum, *Applied Surface Science* **2016**, *362*, 406.

[33] S. Tang, T. Liu, Q. Dang, X. Zhou, X. Li, T. Yang, Y. Luo, E. Sharman, J. Jiang, *J. Phys. Chem. Lett.* **2020**, *11*, 5051.

[34] Z. Jin, C. Liu, Z. Liu, J. Han, Y. Fang, Y. Han, Y. Niu, Y. Wu, C. Sun, Y. Xu, *Adv. Energy Mater.* **2020**, *10*, 2000797.

[35] J. Xia, S.-Z. Yang, B. Wang, P. Wu, I. Popovs, H. Li, S. Irle, S. Dai, H. Zhu, *Nano Energy* **2020**, *72*, 104681.

[36] J. Sun, W. Kong, Z. Jin, Y. Han, L. Ma, X. Ding, Y. Niu, Y. Xu, *Chinese Chem. Lett.*, **2020**, *31*, 953

[37] Z. Li, Y. Wu, *Small* **2019**, *15*, 1804736.

Entry for the Table of Contents
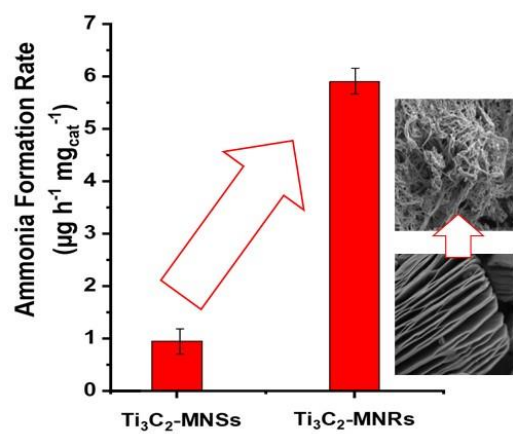
Transformation of Ti_3C_2 MXenes from 2D (nanosheets) to 3D (nanoribbon) enhances significantly the N_2 electrocatalytic conversion rate to NH_3.